Deformation and toughness of polymeric systems: 2. Influence of entanglement density

M. C. M. van der Sanden*, H. E. H. Meijer and T. A. Tervoort
Centre for Polymers and Composites (CPC), Eindhoven University of Technology, PO Box 513, 5600 MB Eindhoven, The Netherlands
(Received 28 October 1992)

In part 1 of this series, the concept of a critical material thickness was introduced and demonstrated experimentally using polystyrene (PS) as a test material. Below the critical thickness, brittle polymers become ductile. The value of the critical thickness is material-dependent and related to the entanglement density. The dependence of the critical thickness on the entanglement density was investigated using the miscible system polystyrene–poly(2,6-dimethyl-1,4-phenylene ether) (PS–PPE). PS possesses a low entanglement density and PPE a high entanglement density, and the system's entanglement density can be varied depending on the relative ratio of PS and PPE in the mixture. Equivalent to the experimental procedure developed in our previous paper, the thickness was set by either changing the PS–PPE layer thickness in stratified PS–PPE/PE tapes (polyethylene (PE) is present to separate the PS–PPE layers) or by adjusting the volume fraction of non-adhering core–shell rubbery particles in the PS–PPE blend, i.e. the ligament thickness. The experimentally determined critical thickness (ID_c) proved to increase continuously from 0.06 μm for PS–PPE 80–20 to 0.18 μm for PS–PPE 40–60 blends. This compares well with the value of 0.05 μm found for pure PS. Under the (moderate) testing conditions used, the PS–PPE 20–80 blend was always tough. The maximum macroscopic strain to break (λ_{macr}) of the PS–PPE blends correlated with the theoretical value (λ_{max}) based on stretching the entanglement network to its full extension. The transition from a macroscopic, brittle-to-ductile deformation behaviour is associated with a change in type of deformation mechanism from void formation (e.g. crazing) to shearing, except for the PS–PPE 20–80 blend, which always deforms by shear deformation. A simple model based on an energy criterion could explain the occurrence of a critical material ligament thickness as well as its dependence on the entanglement density.

(Keywords: deformation; toughness; entanglement density; critical thickness; polystyrene; poly(2,6-dimethyl-1,4-phenylene ether); blends)

INTRODUCTION

In part 1 of this series[1] it was shown that the macroscopic deformation and toughness of amorphous polymers, which suffer from catastrophic strain localizations, can be controlled by changing the microstructure. The concept of a material-specific critical thickness, either in the form of thin sheets in stratified structures (with a non-adhering polymer acting as a spacer) or as ligaments separated by 'holes', was verified for polystyrene (PS). For PS, with ligaments of a (local) thickness of 0.05 μm, the maximum macroscopic strain at break was found to be 200%, about 60% of the theoretical maximum strain at break (320%). Kramer *et al.*[2,3] observed the same deviation between the (maximum) natural draw ratio (λ_{max}) of a *shear-deforming* polymer and the local strain level inside a plane-stress deformation zone (λ_{DZ}). They analysed a large number of amorphous polymers (classified by entanglement molecular weight, M_e) and found in all cases a constant ratio $\lambda_{DZ}/\lambda_{max}=0.6$. Their explanation for the discrepancy between the expected and the experimentally determined value is associated with the rather naive character of the model[2,3], which is based on the maximum extension of a *single* entanglement strand only.

In order to extend the maximum strains from the distinct localizations in crazes and shear bands to the macroscopic level, the stress in the deformed regions should not surpass the breaking stress, while the stress in the connected undeformed material should be higher than the yield stress. From this qualitative explanation for the existence of a critical material thickness, a dependence of this thickness on the maximum extension ratio and thus on the network or entanglement density is to be expected. This aspect of the deformation behaviour of polymers was investigated in this study, combined with the influence of entanglement density on the final macroscopic strain to break.

The system polystyrene–poly(2,6-dimethyl-1,4-phenylene ether) (PS–PPE) was chosen as a model system because for this miscible pair of amorphous polymers[4,5] the entanglement density can be varied by adjusting the relative volume fractions of both constituents[6]. Results of both multilayered tapes of PS–PPE/PE (thin films of PS–PPE alternating with polyethylene (PE)) as well as non-adhering core–shell rubber-modified materials (thin

* To whom correspondence should be addressed

0032-3861/93/142961-10

matrix ligaments) will be discussed, although the detailed analysis of multilayered PS–PPE/PE tapes is postponed to a future paper[7]. Via dilatometry the competition between crazing and shear deformation was investigated and, finally, a simple model will be proposed to explain the relationship between the critical thickness and the entanglement density.

EXPERIMENTAL

Materials

The materials used were polystyrene (Dow, Styron 638), poly(2,6-dimethyl-1,4-phenylene ether) (General Electric Co., PPE-803), low-density polyethylene (DSM, LDPE 1808 AN) and a core–shell rubber possessing a poly(methyl methacrylate) shell and a styrene–butadiene core (Rohm and Haas Co., Paraloid EXL 3647). The PS was a general-purpose extrusion grade: d.s.c., $T_g = 88°C$; g.p.c. ($CHCl_3$), $M_n = 70\,kg\,mol^{-1}$ and $M_w = 200\,kg\,mol^{-1}$. The PPE was used as received: d.s.c., $T_g = 215°C$; $IV = 0.37\,dl\,g^{-1}$ ($CHCl_3$, 25°C); g.p.c. ($CHCl_3$), $M_n = 14.3\,kg\,mol^{-1}$ and $M_w = 31.5\,kg\,mol^{-1}$. The PE was an injection-moulding type possessing a melt flow index of $7.5\,dg\,min^{-1}$. The core–shell rubber was an extrusion grade and the size of the rubbery particles was in the range of 0.1–0.3 μm.

Sample preparation

PS and PPE were compounded in various weight fractions (PS–PPE 80–20, 60–40, 40–60 and 20–80) in order to obtain blends with various entanglement densities. Extrusion was carried out on a co-rotating twin-screw extruder (Werner and Pfleiderer ZSK 25) with a standard screw geometry. A master batch of PS–PPE 50–50 was prepared at 290°C. This master batch was used to prepare the PS–PPE 80–20 and 60–40 blends during a second extrusion cycle, at respectively 250 and 270°C (the extrusion temperature was kept as low as possible in order to avoid (any) degradation of the PPE). The PS–PPE 40–60 and 20–80 blends were prepared during a double extrusion cycle at 290°C.

Multilayered PS–PPE/PE samples were prepared using a Multiflux static mixer[8,9]. The principle of this mixer was described in part 1 of this series[1]; however, in this study an improved version of the previously introduced Multiflux mixer was used. Thin laminated tapes consisting of alternating layers of PS–PPE and PE were prepared at respectively 220°C (PS–PPE 80–20), 225°C (PS–PPE 60–40) and 230°C (PS–PPE 40–60) and contained a varying number of layers: from 128 (six mixing elements) up to 4096 (11 mixing elements). PS–PPE and PE were applied in three different proportions: 75/25, 50/50 and 25/75 w/w. Small dumbbell-shaped tensile specimens were machined from these tapes parallel to the direction of extrusion according to ASTM D 1708 (the thickness was kept constant around 0.3 mm).

Core–shell rubber-modified PS–PPE blends containing 10, 20, 30, 40, 50 and 60 wt% rubber were prepared in a two-step compounding process, as described above. During the second extrusion step the core–shell rubber was added (processing temperatures are shown in *Table 1*).

Extruded strands were quenched and pelletized subsequently. Both the neat and the rubber-modified PS–PPE blends were injection moulded (Arburg Allrounder 220-75-250) into dog-bone-shaped tensile bars (DIN 53 455, sample thickness 3 mm). The temperature at which the injection moulding was carried out depended on the blend composition and is listed in *Table 1* for the various PS–PPE blends.

Table 1 Processing temperatures for the various neat and rubber-modified PS–PPE blends

Blend composition[a]	Processing temperature (°C)
80–20/X[b]	250
60–40/X	270
40–60/X	290
20–80/X	290

[a] The blend composition is indicated with a three-number code: 'weight fraction PS present in the matrix'–'weight fraction PPE present in the matrix'/'weight fraction core–shell rubber present in the total blend ($=X$)'

[b] The processing temperature was, independently of the rubber concentration, only determined by the matrix composition

Mechanical testing

Prior to mechanical testing, the layered samples as well as the injection-moulded tensile bars were annealed at a temperature 20°C below the glass transition temperature of the matrix for at least 24 h.

The layered samples and the core–shell rubber-modified tensile specimens were uniaxially strained on a Frank tensile machine (type 81565 IV) at a cross-head speed of $5\,mm\,min^{-1}$ at room temperature. To obtain accurate data concerning the longitudinal strain level of the specimens, extensometers were used in the latter case. At least five specimens were fractured for each testing condition.

In order to obtain data on the relative volume change ($\Delta V/V_0$) of a (core–shell rubber-modified) PS–PPE blend during tensile loading, tensile dilatometry was used[10]. This technique not only allows determination of the mechanical characteristics of a material (e.g. Poisson's ratio), but can also be used to obtain information on the type of deformation mechanism. Tensile dilatometry, as applied in this investigation, is extensively described in ref. 1.

Dynamic mechanical thermal analysis

The storage shear modulus of neat PS–PPE blends was determined in the melt as a function of the angular frequency (10^{-2}–$10^{2}\,rad\,s^{-1}$) for at least five different temperatures over a range of 50°C, using a Rheometrics RDS II spectrometer. A plate–plate geometry was used (diameter 25 mm) at a maximum strain of 2%. The thickness of the samples was 1 mm. Shifting of the G' *versus* ω curves to a reference temperature, approximately 40°C above the glass transition temperature, resulted in a master curve. The rubber plateau modulus G_{N0} is equal to the storage modulus G' at the frequency where $\tan\delta$ is at its minimum in the plateau zone of the master curve[11,12]. Applying the classical concept of rubber elasticity theory, the molecular weight between entanglement nodes, M_e, could be calculated[13]:

$$M_e = \rho RT/G_{N0} \quad (1)$$

where ρ is the density, R is the gas constant and T is the reference temperature.

Scanning electron microscopy

Scanning electron microscopy (SEM; Cambridge Stereo Scan 200) was applied to check the continuity of the layers in PS–PPE/PE tapes and the homogeneity of the rubber particle distribution in core–shell rubber-modified PS–PPE blends. Specimens were cut from respectively the centre of the layered specimen, parallel to the direction of extrusion and perpendicular to the layers, and from the centre of the injection-moulded tensile bar, again parallel to the direction of extrusion. The surface of the samples was microtomed using a glass knife at liquid-nitrogen temperature, in order to avoid any deformation during sample preparation. After microtoming, the sample was etched in an oxygen plasma to remove the polyethylene, respectively the rubbery particles, and to gain more contrast. Finally, the samples were covered with a conducting gold layer.

In order to investigate the deformation and fracture characteristics of the core–shell rubber-modified tensile specimens, post-mortem fracture surface analysis was carried out using SEM. For this purpose, the specimens were not etched in an oxygen plasma, but were directly covered with a gold layer.

D.s.c. measurements

Glass transition temperatures of extruded neat PS–PPE blends were recorded using a Perkin–Elmer DSC-7 differential scanning calorimeter. The samples were first heated to 250°C, quenched from the melt to ambient temperature and then scanned at a standard heating rate of 20°C min^{-1}. Indium was used for temperature calibration ($T_{m,onset}$ = 156.6°C). The glass transition temperatures (T_g) were determined using the intercept of the tangent at the point of maximum slope and the extrapolated baseline on the low-temperature side of the transition.

RESULTS AND DISCUSSION

Characterization of layered PS–PPE/PE tapes and (rubber-modified) PS–PPE blends

Table 2 shows T_g values of PS–PPE blends after extrusion and injection moulding as revealed by d.s.c. For all blend compositions only a single T_g value is observed, clearly confirming the miscibility of PS and PPE on a molecular scale[4,5].

The master curves of the PS–PPE 100–0, 80–20 and 60–40 blends as obtained from dynamic mechanical thermal analysis are shown in *Figure 1*. The master curves for the PS–PPE 40–60 and 20–80 blends are omitted because these samples showed void formation during measuring at the required high temperatures, indicating thermal degradation of the samples. The temperatures to which the master curves are shifted are respectively 130, 145 and 160°C (T_g + 40°C) for the PS–PPE 100–0, 80–20 and 60–40 blends. It is clear from *Figure 1* that an increase of the PPE content in the PS–PPE blends results in a shift of the G' curve to higher values. The rubber plateau modulus is determined at the minimum of tan δ in the plateau region and is used to calculate the molecular weight between entanglement nodes using equation (1). The entanglement density (ν_e) can be calculated using[3]:

$$\nu_e = \rho N_A / M_e \qquad (2)$$

where N_A is Avogadro's number.

In *Figure 2* the value of the entanglement density is plotted *versus* the PS–PPE composition (filled squares). Prest and Porter[6] have determined the entanglement density for several PS–PPE blends as well. They experimentally derived an equation to describe the entanglement molecular weight as a function of the blend composition:

$$M_e(\chi) = \frac{M_e(\mathrm{PS})}{(1 + 3.2\chi)} \qquad (3)$$

where χ is the weight fraction of PPE in the blend and M_e(PS) is the entanglement molecular weight of

Table 2 Glass transition temperatures for neat PS–PPE blends

Blend composition	Glass transition temperature (°C)
80–20	105
60–40	123
40–60	144
20–80	174

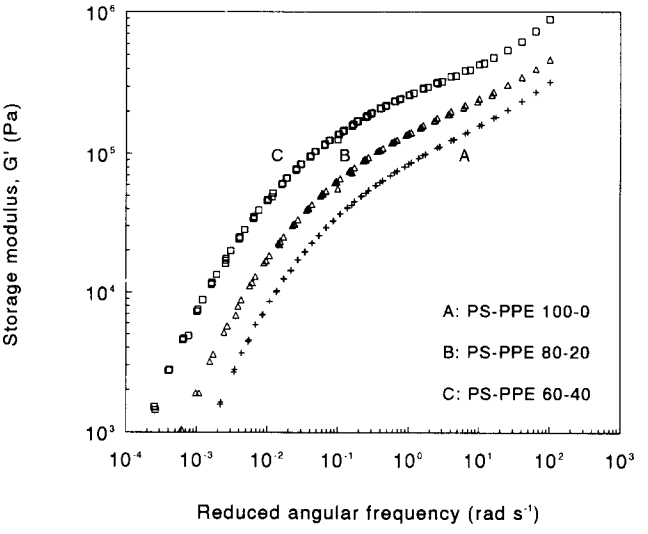

Figure 1 Master curves of PS–PPE blends ((A) 100–0, (B) 80–20 and (C) 60–40) as obtained from dynamic mechanical thermal analysis (reference temperatures are respectively 130, 145 and 160°C)

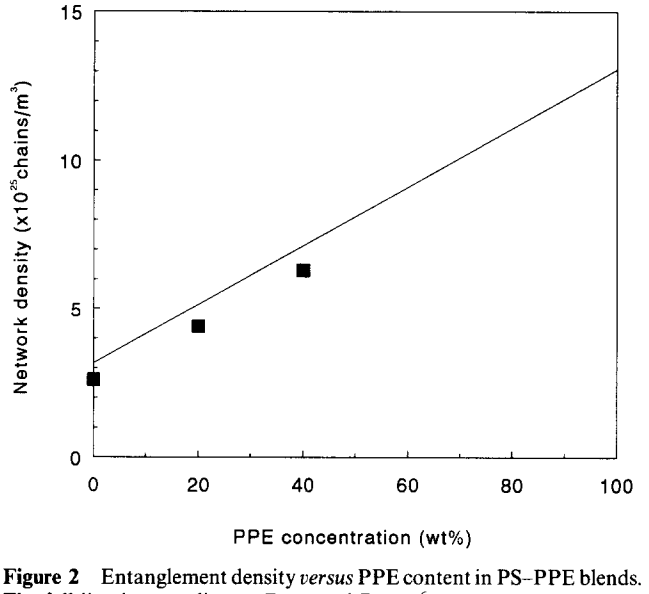

Figure 2 Entanglement density *versus* PPE content in PS–PPE blends. The full line is according to Prest and Porter[6]

polystyrene[14], $M_e(PS) = 19.1\ kg\ mol^{-1}$. Although Prest and Porter derived this equation for a limited range of blend compositions ($0 < \chi < 0.4$) the equation is assumed to be valid up to $\chi = 0.8$. Values of v_e for the various PS–PPE compositions are calculated by combining equations (2) and (3). The results of these calculations are also shown in *Figure 1* (full line). As can be inferred from this figure the entanglement density as obtained from our rheological measurements corresponds well with the values as obtained from data of Prest and Porter. The entanglement density varies linearly between the values of pure PS (3.2×10^{25} chains/m^3) and of pure PPE (13.2×10^{25} chains/m^3).

In *Figure 3* SEM micrographs are shown of various microtomed multilayered PS–PPE/PE tapes. The continuity of the layers is clear for *Figures 3a* and *3c* and only a small variation in layer thickness can be observed. For the PS–PPE/PE 25/75 w/w tape (PS–PPE 80–20, 11 mixing elements, *Figure 3b*), however, the layer continuity is clearly absent. Obviously, the PS–PPE composition (read:viscosity ratio of PS–PPE/PE) has a large influence on the maximum number of mixing elements possible to apply in the Multiflux mixer before layer discontinuity occurs (compare *Figures 3b* and *3c*). (For pure PS[1], tapes consisting of continuous layers could only be obtained if the number of mixing elements in the previously used Multiflux static mixer did not exceed six.)

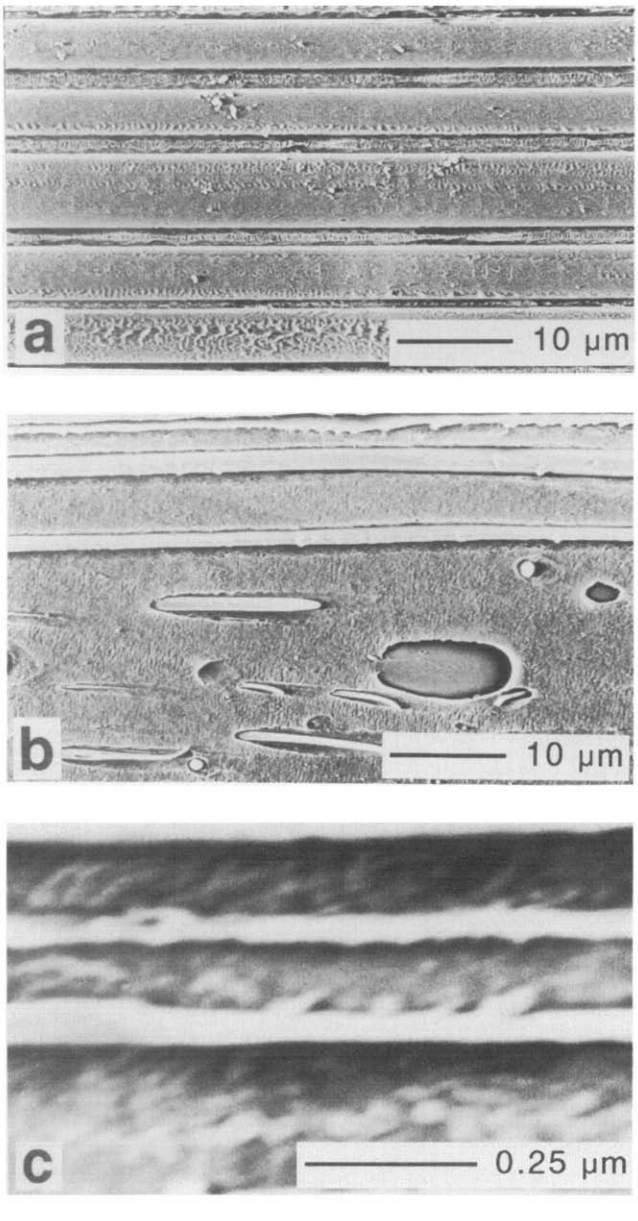

Figure 3 SEM micrographs of multilayered PS–PPE/PE tapes: (a) PS–PPE/PE 75/25 (PS–PPE 80–20), six mixing elements, (b) PS–PPE/PE 25/75 (PS–PPE 80–20), 11 mixing elements and (c) PS–PPE/PE 25/75 (PS–PPE 60–40), 11 mixing elements

A selection of various microtomed injection-moulded rubber-modified PS–PPE blends is shown in *Figure 4*. For the lower rubber concentrations (*Figure 4a*, PS–PPE/rubber 80–20/20 blend) the particle distribution shows a moderate degree of orientation of the particles parallel to the direction of mould flow during the injection moulding step. However, for the higher-weight-fraction core–shell rubber the particle distribution is fairly homogeneous (*Figures 4b* and *4c*). If the matrix consists of PS–PPE 20–80, however, a homogeneous particle distribution is already obtained for the lower rubber concentrations (see *Figures 4d* and *4e*). However, the particles seem to be coagulated to a small extent for the PS–PPE 20–80 blends.

Mechanical properties of multilayered PS–PPE/PE tapes

In a future paper a more extended discussion of the deformation behaviour and mechanical properties of PS–PPE/PE tapes will be given[7]. Here, only a few results of the multilayered systems will be presented in order to compare these with data obtained from core–shell rubber-modified PS–PPE blends.

In *Figure 5* the strain to break of stratified tapes is plotted *versus* PS–PPE layer thickness for PS–PPE 60–40 and 40–60 blends. As can be inferred from *Figure 5* (PS–PPE 60–40), the strain to break increases with decreasing layer thickness. The experimentally achievable maximum strain at break (about 70%) is observed for the thinnest PS–PPE layers (PS–PPE/PE 25/75, 11 mixing elements). A further decrease in layer thickness, by an increase in number of mixing elements, results in a discontinuous layer structure.

For PS–PPE 40–60 (*Figure 5*) the thickness below which an increase in strain at break is observed is located at a higher level ($\approx 0.25\ \mu m$) compared to PS–PPE 60–40 ($\approx 0.06\ \mu m$). Thus, a pronounced influence of the entanglement density is found. For the PS–PPE 40–60 blend, the maximum level of strain at break attainable in the ductile region can be estimated to be 70%.

In contrast to pure PS[1], which only showed the onset of an increase in strain at break with stratified structures, the PS–PPE 40–60 blend seems to reach its maximum macroscopic strain, and thus the true critical thickness is found. It is, therefore, even more interesting to compare these data with the more practical 'holey' structures obtained by adding non-adhering core–shell rubbers.

Mechanical properties of rubber-modified PS–PPE blends

Strain to break. Strain-to-break data, obtained from slow-speed ($5\ mm\ min^{-1}$) tensile tests of various rubber-modified PS–PPE blends, are shown in *Figure 6*. The data for PS[1] (*Figure 6*, curve A) are taken as a reference. If 20 wt% PPE is added to PS, the strain to break as a function of the rubber concentration (*Figure 6*, curve B) shows, analogous to PS, a steep increase with increasing rubber weight fraction. However, in this case the

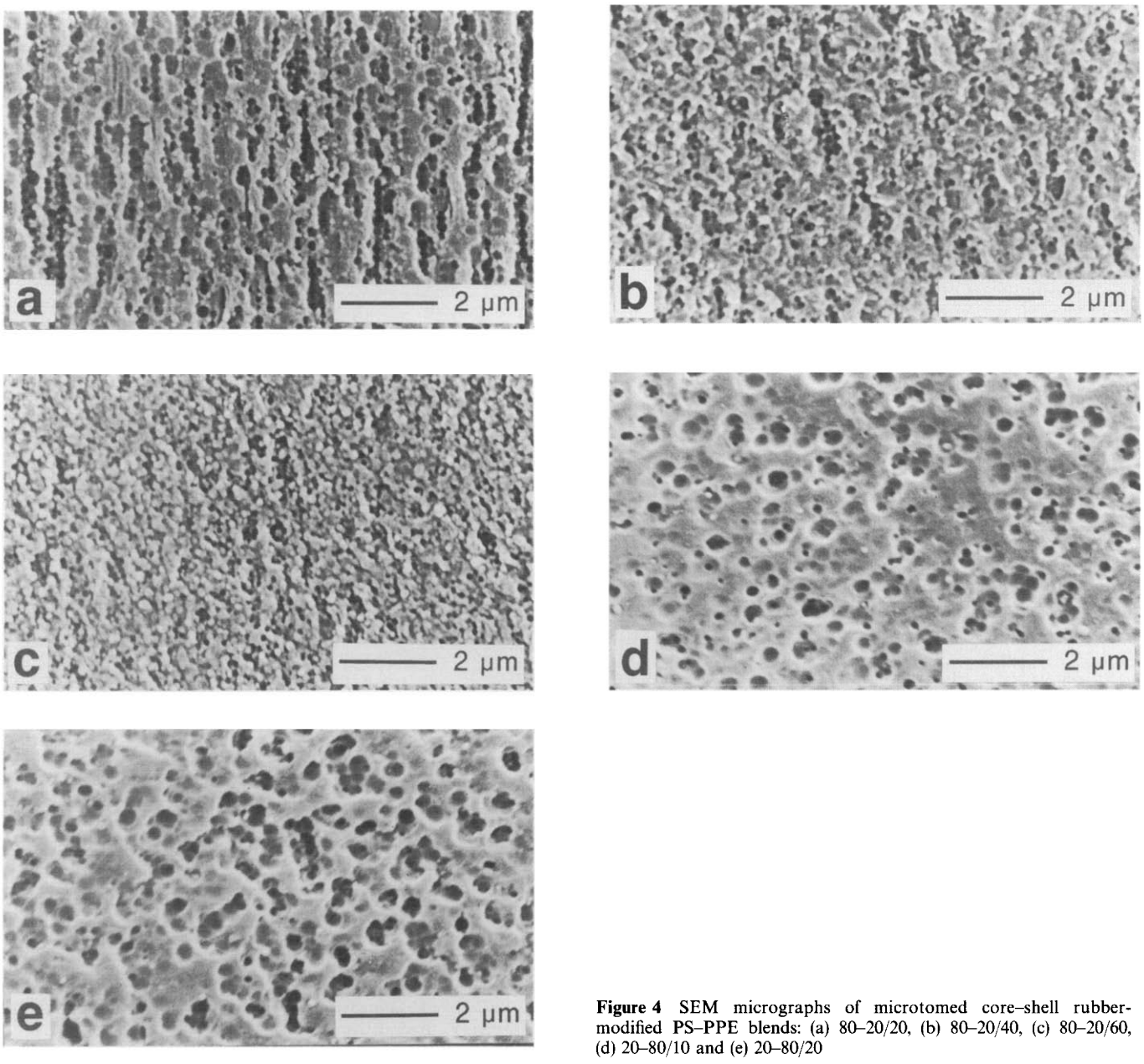

Figure 4 SEM micrographs of microtomed core–shell rubber-modified PS–PPE blends: (a) 80–20/20, (b) 80–20/40, (c) 80–20/60, (d) 20–80/10 and (e) 20–80/20

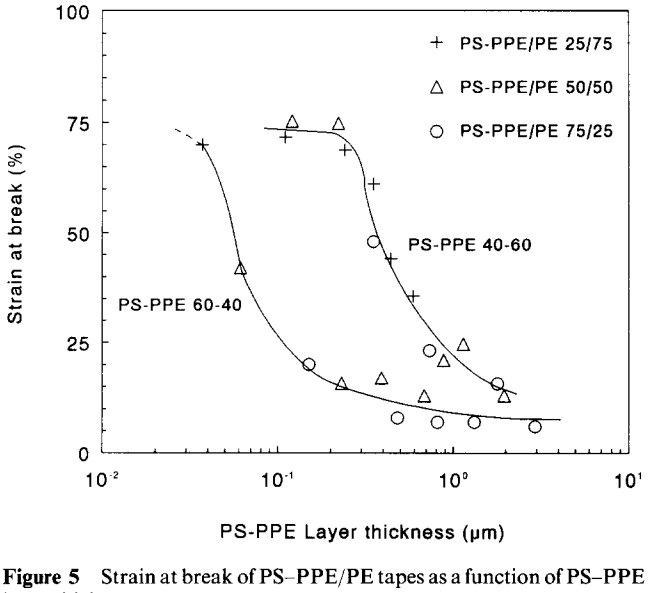

Figure 5 Strain at break of PS–PPE/PE tapes as a function of PS–PPE layer thickness

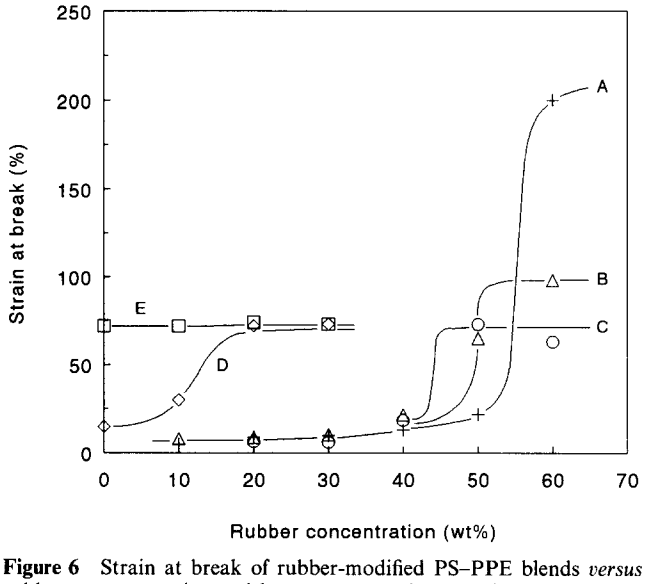

Figure 6 Strain at break of rubber-modified PS–PPE blends *versus* rubber concentration with parameter the matrix composition (PS–PPE): (A) 100–0, (B) 80–20, (C) 60–40, (D) 40–60 and (E) 20–80

transition already occurs at a lower rubber concentration (50 wt%), i.e. a higher ligament thickness compared to PS. The maximum value of the strain to break in the 'tough region' is about 100% and considerably lower than the value for core–shell rubber-modified blends having a pure PS matrix (strain at break of approximately 200%).

Curves C and D in *Figure 6* clearly confirm this trend. With an increasing PPE content in the matrix, two phenomena are observed: (i) the critical ligament thickness is positioned at a lower rubber concentration and (ii) the maximum value of the strain to break in the ductile region decreases (for curves C and D the levels of strain to break in the tough region are equal). Notice that the strain to break in the ductile region of the core–shell rubber-modified PS–PPE 60–40 and 40–60 blends coincides with the maximum strain to break observed for the corresponding PS–PPE/PE tapes. For the PS–PPE 20–80 blend all samples show a macroscopic strain to break of about 65%, independently of the rubber weight fraction (*Figure 6*, curve E). Clearly, no brittle-to-ductile transition is found in the given test range. As will be shown in a future paper, PS–PPE 20–80 blends can demonstrate a brittle-to-ductile transition under more extreme testing conditions (tensile speed 1 m s^{-1}, notched)[15].

Tensile dilatometry. To analyse the type of deformation mechanism operative in the various core–shell rubber-modified PS–PPE blends, slow-speed tensile dilatometry is carried out (*Figures 7, 8* and *9*). If PS–PPE 80–20 forms the matrix phase the slope of the $\Delta V/V_0$ curve goes to unity if the rubber concentration is 20 wt% or less (*Figure 7*), indicating a process of void formation during elongation. Void formation can be either the result of the continuation of further detachment of the rubbery particles from the matrix phase or the result of the crazing mechanism normally operative in this blend[16]. However, if the rubber weight fraction is increased to 50 wt% the slope decreases to zero after passing the elastic region (0–1.5% strain). This clearly indicates a shear deforming mechanism to be operative in the blend during longitudinal elongation. The transition from a deformation mechanism accompanied by void formation to a shear deforming mechanism occurs at the same

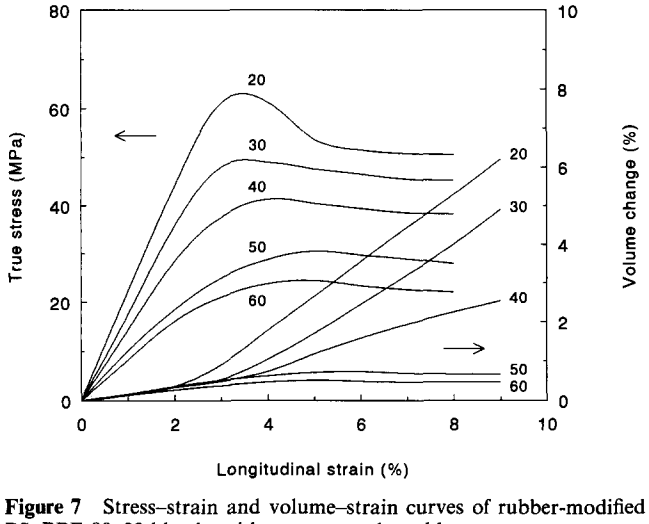

Figure 7 Stress–strain and volume–strain curves of rubber-modified PS–PPE 80–20 blends, with parameter the rubber content

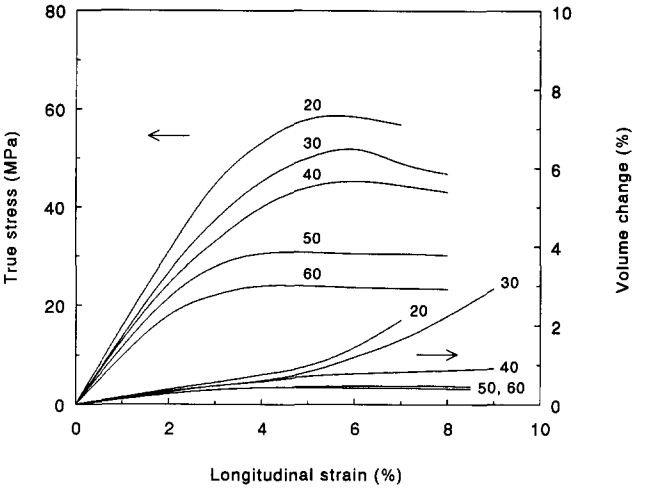

Figure 8 As *Figure 7*, for PS–PPE 60–40 blends

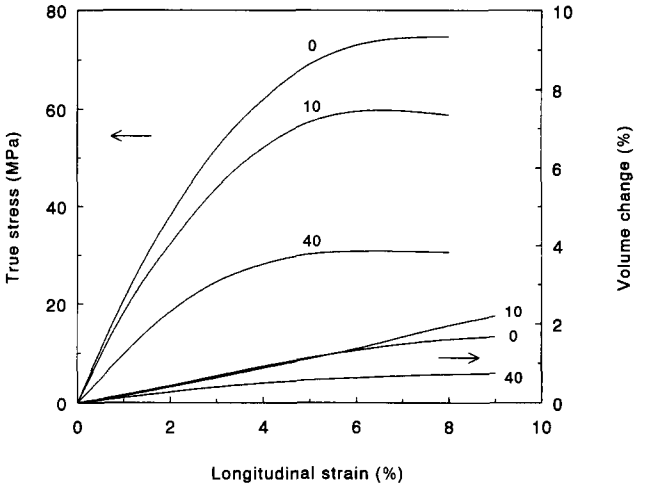

Figure 9 As *Figure 7*, for PS–PPE 20–80 blends

rubber concentration (50 wt%) as the sudden increase in strain to break as shown in *Figure 6*, curve B.

The results of the dilatometry experiments for PS–PPE 60–40 core–shell rubber-modified blends are shown in *Figure 8*. If the rubber concentration is below the critical level (see *Figure 6*, curve C: 20, 30 and 40 wt% rubber) deformation is always accompanied by an increase in volume strain, while in the ductile region pure shear deformation is observed. Analogous to the PS–PPE 80–20 blend the transition from brittle to ductile deformation behaviour occurs simultaneously with the transition from a deformation mechanism accompanied by void formation to a shearing type of deformation.

For the neat PS–PPE 20–80 blend the slope of the $\Delta V/V_0$ curve (*Figure 9*, 0 wt% core–shell rubber) decreases to zero after passing the elastic region, confirming that shear deformation occurs in this blend during longitudinal elongation, as also reported in the literature[17,18]. If 10 wt% core–shell rubber is present, the $\Delta V/V_0$ curve shows a moderate increase in slope after exceeding 4% longitudinal strain. This is probably the consequence of detachment of the rubbery particles upon increase in strain level since even in the neat blend shear deformation was demonstrated to occur. The slope of the $\Delta V/V_0$ curve corresponding to 40 wt% rubber (*Figure 9*)

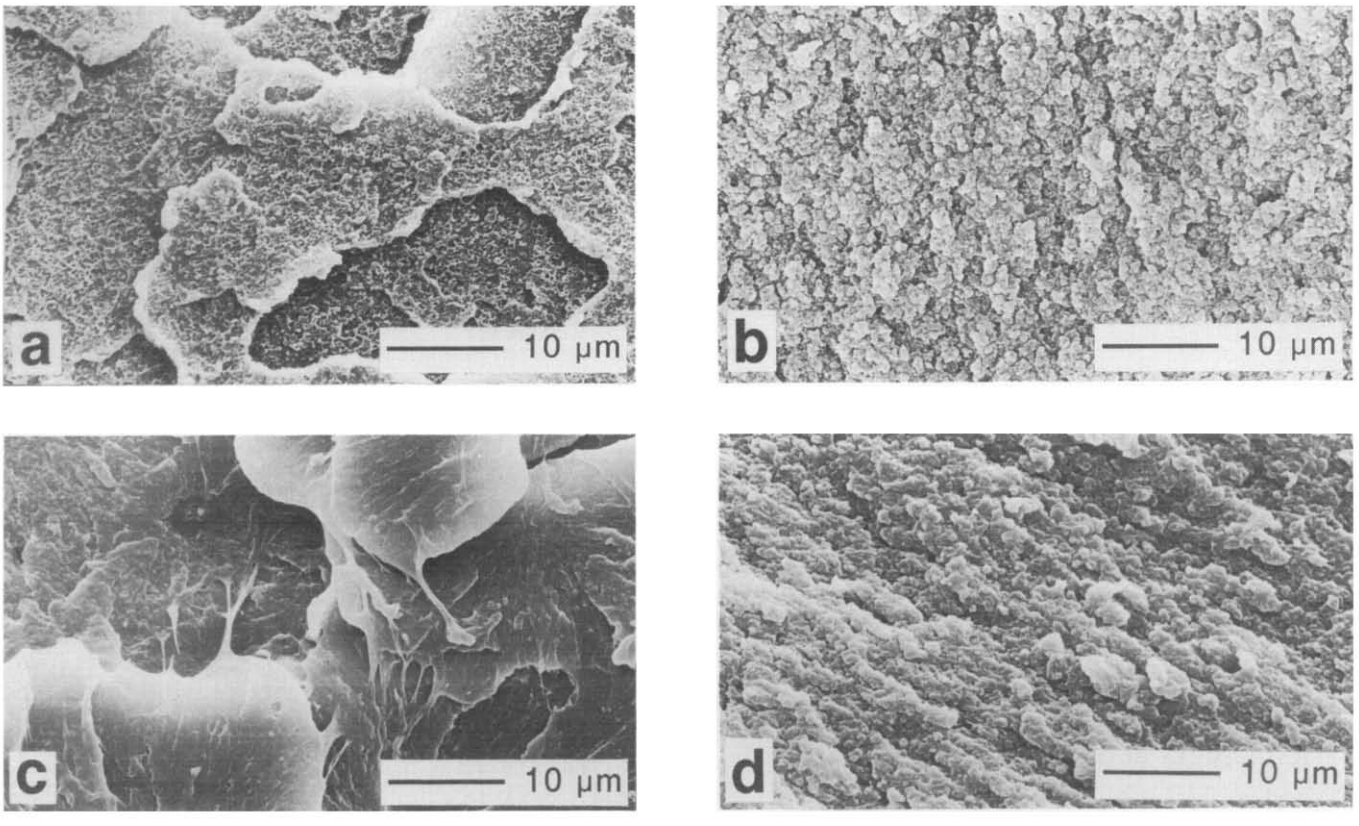

Figure 10 SEM micrographs of fracture surfaces of rubber-modified PS–PPE blends: (a) 80–20/20, (b) 80–20/60, (c) 20–80/0 and (d) 20–80/20

decreases to zero after passing the elastic region, again demonstrating the shear deformation mechanism to be operative.

Fracture surfaces

Figure 10 shows SEM micrographs of fracture surfaces of various PS–PPE 80–20 and 20–80 blends, uniaxially strained at 5 mm min^{-1}. For the 80–20/20 mixture a brittle fracture surface is observed (*Figure 10a*). Clearly, the fracture surface is influenced by the presence of the non-adhering rubbery particles, which act as potential crack initiators. If 60 wt% core–shell rubber is added to the PS–PPE 80–20 matrix, extensive ductility can be observed on the fracture surface (*Figure 10b*). The PS–PPE 20–80 blend, on the other hand, shows even ductility on the fracture surface without rubber toughening (*Figure 10c*). Addition of 20 wt% rubbery particles does not change the fracture surface considerably: the level of ductility remains about the same (*Figure 10d*).

THEORETICAL CONSIDERATIONS

Macroscopic strain

The maximum extension ratio of an entanglement network can be calculated using the classical theory of rubber elasticity[19]. In *Figure 11* the experimentally determined maximum macroscopic strain to break (λ_{macr}) of the various multilayered and rubber-modified PS–PPE blends is shown as a function of the theoretical maximum extension ratio (λ_{max}) of the entanglement network of the PS–PPE phase. As can be inferred from *Figure 11*, the experimentally determined values correlate well with results of Kramer *et al.* on strain levels determined *locally*

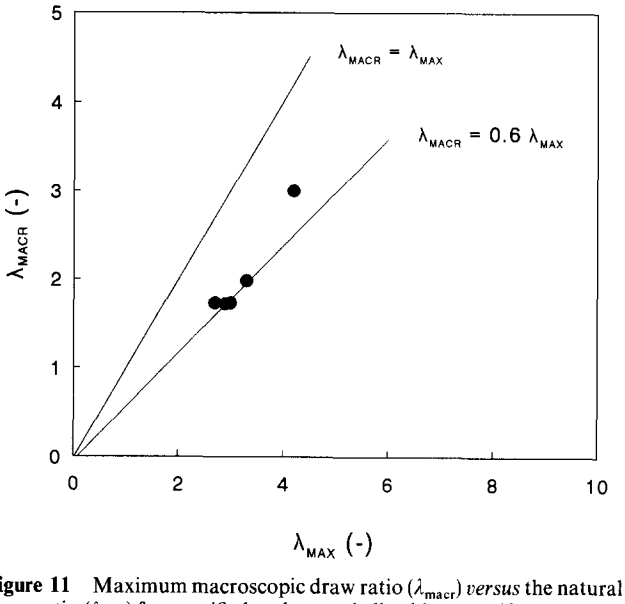

Figure 11 Maximum macroscopic draw ratio (λ_{macr}) *versus* the natural draw ratio (λ_{max}) for stratified and core–shell rubber-modified PS–PPE blends

inside a deformation zone[2,3] ($\lambda_{DZ}=0.6\lambda_{max}$). The reason for the discrepancy between the theoretical value, λ_{max}, and λ_{DZ} (or λ_{macr}) must be related to the non-ideal character of the entanglement network and the assumption of taking one single entanglement strand in order to estimate the theoretical extension ratio of a three-dimensional entanglement network, as already discussed in the 'Introduction'.

The macroscopic strain-to-break data of *Figure 11* can be presented as a function of the entanglement density

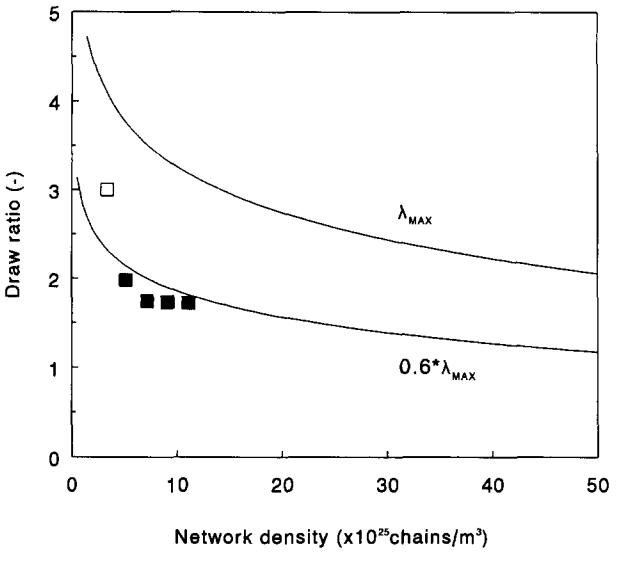

Figure 12 Draw ratio *versus* network density (entanglement and/or crosslink density). For details, see text

(see *Figure 12*) to yield the overall picture of deformation and toughness of amorphous polymers. The filled squares correspond to data obtained from multilayered and rubber-modified PS–PPE blends, and the open square corresponds to PS[1]. In part 3 of this series[20] the right-hand side of this figure will be investigated, using thermosets of varying crosslink density.

Critical microscopic thickness

The rubber weight fraction at which a sharp increase in strain to break is observed for rubber-modified PS–PPE blends (*Figure 6*) corresponds to a certain average surface-to-surface interparticle distance, *ID* (read:ligament thickness), which can be calculated from the rubber particle size and volume fraction (assuming a body-centred-cubic lattice)[21–23]. It can be inferred from *Figure 6* that the critical ligament thickness increases with increasing PPE content present in the matrix (analogous to multilayered PS–PPE/PE tapes; see *Figure 5*). In order to derive a simple first-order model describing the phenomenon of the thickness-dependent brittle-to-ductile transition, the conditions have to be investigated that allow for a continuation of local deformation without fatal fracture. A lattice of holes, which is a schematic representation of non-adhering rubbery particles in a PS–PPE matrix, creates thin ligaments of polymeric material, i.e. potential initiation places of deformation. The smallest size of a fracture surface is the stretched fibril originating from the matrix ligament between two neighbouring particles. Brittle fracture can only occur if the stored elastic energy per matrix ligament is larger than the energy needed to create a brittle fracture of this fibril. The stored elastic energy per ligament can be considered to be correlated with the volume of matrix material that is relieved from elastic stress if a brittle fracture were to occur in the connecting fibril. Although only detailed micromechanical analysis in a substantial volume around a matrix filament could give conclusive answers on the elastic energy stored in the volume that is released after the rupture of the fibril, a rough first approximation could be the matrix volume between two holes: see the shaded area in *Figure 13a* (direction 1 is the direction of the applied stress). This volume can be estimated to be a sphere, having a diameter of d_1 ($=h$). The maximum average stress in this volume is estimated to be the yield stress, σ_y, since higher stresses would result in ductile plastic deformation of the ligament. The *available* elastic energy, U_{av}, per ligament is therefore:

$$U_{av}=\frac{\pi}{6}(d_1)^3\frac{\sigma_y^2}{2E_1} \tag{4}$$

where E_1 is the Young's modulus of the PS–PPE blend. The energy *required* to create a brittle fracture, U_{re}, can be estimated to be:

$$U_{re}=2\frac{\pi}{4}(d_2)^2\Gamma \tag{5}$$

where Γ is the surface energy of the polymeric matrix material. The size of a possible fracture surface (diameter d_2, *Figure 13b*) is proportional to the original cross-sectional area of the matrix ligament divided by λ_{max}, since this is the most critical condition, analogous to the use of the yield stress in equation (4). The surface energy is given by[3]:

$$\Gamma=\gamma+\tfrac{1}{4}v_e dU \tag{6}$$

where γ is the van der Waals surface energy, d is the root-mean-square end-to-end distance between junction points in the network and U is the polymer backbone bond energy (the influence of a moderate degree of molecular orientation on the value of the surface energy is neglected). According to Kramer *et al.*[3], $v_e d$ scales roughly as $v_e^{1/2}$ (the polymer backbone bond energy is roughly equal for all amorphous polymers). Combining equations (4), (5) and (6) results in an energy criterion for the brittle-to-ductile transition:

$$d_1=ID_c=\frac{6(\gamma+k_1 v_e^{1/2})E_1}{\lambda_{max}\sigma_y^2} \tag{7}$$

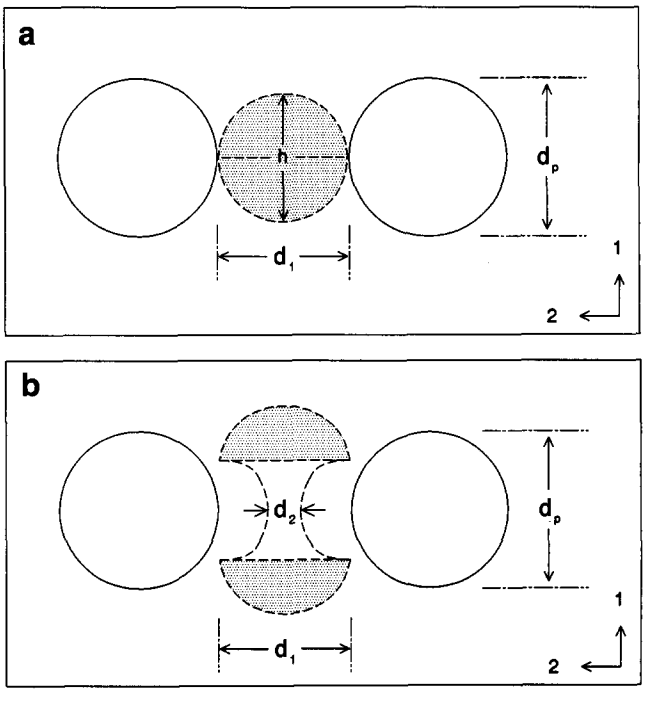

Figure 13 Schematic view of a matrix ligament betwen two holes, representing non-adhering rubbery particles: (a) before plastic deformation and (b) during plastic deformation. The shaded area represents the elastically deformed volume that is relieved from elastic stress once the fibril breaks

If the value of ID is larger than ID_c ('critical interparticle distance'), brittle fracture of the ligament is possible ($U_{av} > U_{re}$) and therefore will occur. If, on the other hand, $ID < ID_c$, brittle fracture cannot occur ($U_{av} < U_{re}$) and complete deformation of the ligament will take place, eventually leading to a fully ductile macroscopic fracture behaviour.

Taking for PS, $\gamma = 40\ \text{mJ m}^{-2}$, $k_1 = 7.13 \times 10^{-15}$ J chain$^{-1/2}$ m$^{-1/2}$ (ref. 3), $E_1 = 3.28 \times 10^9$ Pa (ref. 24), $\lambda_{max} = 4.2$ and $\sigma_y = 82.8$ MPa (ref. 24), results in $ID_c = 0.055\ \mu$m (equation (7)), which is surprisingly close to the experimentally determined value[1] (0.05 μm) given the simplicity of the model and the assumptions made of the volume of matrix material released after rupture of the fibril.

Extending the model by introducing the v_e dependence of λ_{max} ($\lambda_{max} = k_2 v_e^{-1/2}$, constant $k_2 = 2.36 \times 10^{13}$ chains$^{1/2}$ m$^{-3/2}$ (ref. 3), results in:

$$d_1 = ID_c = \frac{6(\gamma + k_1 v_e^{1/2}) E_1}{k_2 v_e^{-1/2} \sigma_y^2} \tag{8}$$

In *Figure 14* the calculated value of ID_c is plotted as a function of the entanglement density for several PS–PPE blends. The full curve is drawn according to equation (8), taking for the yield stress a constant value of 70 MPa; the broken curve is also drawn according to equation (8), but taking for the yield stress data published by Kambour[24]. The Young's modulus of the PS–PPE phase is assumed to be independent of the entanglement density ($E_1 = 3.28 \times 10^9$ Pa). In *Figure 14* the experimentally determined values of ID_c for various core–shell rubber-modified PS–PPE blends are given as well (filled squares). The value of ID_c for the PS–PPE 20–80 blend is taken from ref. 15 (high-speed tensile tests). Not only is the slope representing the entanglement density dependence of the critical thickness predicted well by both curves, but also the absolute values of the critical thickness are surprisingly correct taking into account the simplicity of the model and the serious assumptions that have been made.

In *Figure 14* also two data points are shown obtained from multilayered PS–PPE blends (open squares). As already discussed, these data compare well to those obtained from core–shell rubber-modified PS–PPE blends but, surprisingly, they are also close to the predicted values. In the stratified structures the estimation of the volume of matrix material containing elastic energy to create a brittle facture is much more complicated and, moreover, requires a number of assumptions to be made on the development of the deforming parts.

Although the model presented needs refinements in, for instance, the estimation of the released volume containing stored elastic energy, the results are promising towards an understanding of the phenomenon of a brittle-to-ductile transition. Moreover, the influence of testing temperature and testing speed can be incorporated relatively easily via the temperature and strain rate dependences of the yield stress of the matrix.

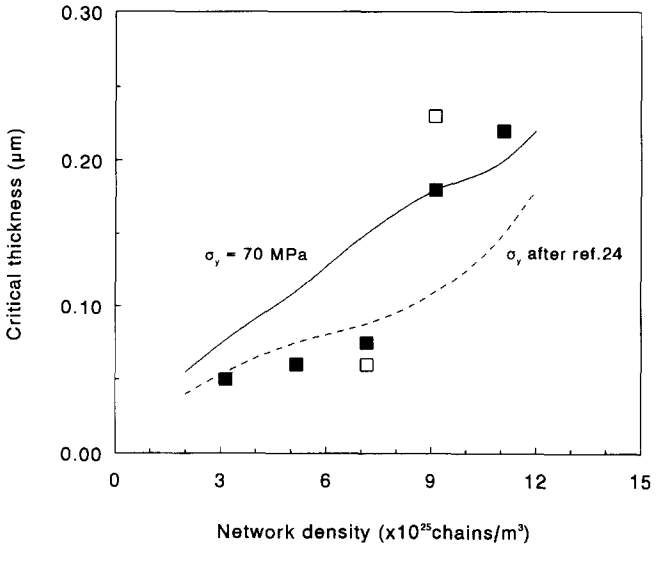

Figure 14 Critical material thickness (ID_c) *versus* the matrix entanglement density (v_e) for the various PS–PPE blends. The curves are according to the model. For details, see text

CONCLUSIONS

The critical thickness below which brittle amorphous glassy polymers become ductile is determined for thin films of PS–PPE (alternating with PE) and for non-adhering core–shell rubber-modified PS–PPE blends in the composition range of 80–20 to 20–80. For the multilayered PS–PPE/PE tapes brittle-to-ductile transitions occurred at 0.06 and 0.3 μm for PS–PPE 60–40 and 40–60 blends respectively. The value of the critical ligament thickness as obtained from core–shell rubber-modified PS–PPE blends varies between 0.06 μm (PS–PPE 80–20) and 0.18 μm (PS–PPE 40–60) for slow-speed tensile testing (5 mm min^{-1}). Under these relatively mild testing conditions the PS–PPE 20–80 blend did not show a brittle-to-ductile transition: the strain to break of this blend was independent of the rubber concentration ($\approx$65%). The strain to break and the critical material thickness as obtained from the multilayered PS–PPE/PE tapes and core–shell rubber-modified PS–PPE blends coincide (at least for the PS–PPE 40–60 blend).

The maximum macroscopic strain to break (λ_{macr}) in the ductile region correlates well with the natural draw ratio (λ_{max}) of the amorphous glass based on its intrinsic entanglement network structure: $\lambda_{macr} = 0.6\lambda_{max}$.

The transition from a brittle to a ductile fracture type of core–shell rubber-modified PS–PPE blends coincides with a transition from a deformation mechanism accompanied by void formation to a shearing type of deformation mechanism for the PS–PPE 80–20 and 60–40 blends, as revealed by tensile dilatometry.

An explanation for the existence of a critical material thickness for 'holey' modified PS–PPE blends is given, based on an energy criterion. This first-order model is verified by the experimental results. Given the simplicity of the model, not only is the qualitative dependence of the critical thickness on network density satisfying, but even the quantitative agreement is surprisingly good. Only a more extended micromechanical stress state analysis around a localized deformed ligament will provide a more solid basis especially for the estimation of the volume that is released upon break-up of the extended fibril. This aspect is still under investigation in our laboratory.

ACKNOWLEDGEMENTS

The authors are grateful to P. G. J. Adriaansen,

F. O. de Bie, L. G. C. Buijs and R. G. M. van Deursen for performing most of the experiments. A. Schepens from DSM Research is acknowledged for his assistance in the injection moulding of various PS–PPE blends. This work was supported by the Foundation for Polymer Blends (SPB).

REFERENCES

1 Van der Sanden, M. C. M., Meijer, H. E. H. and Lemstra, P. J. *Polymer* 1993, **34**, 2148
2 Donald, A. M. and Kramer, E. J. *Polymer* 1982, **23**, 1183
3 Kramer, E. J. and Berger, L. L. *Adv. Polym. Sci.* 1990, **91/92**, 1
4 Fried, J. R., Hanna, G. A. and Kalkanoglu, H. 'Polymer Compatibility and Incompatibility', Harwood Academic, New York, 1982, Vol. 2, p. 237
5 MacKnight, W. J., Karasz, F. E. and Fried, J. R. 'Polymer Blends 1' (Eds. D. R. Paul and S. Newman), Academic Press, San Diego, 1978, 186
6 Prest, W. M. and Porter, R. S. *J. Polym. Sci. (A-2)* 1972, **10**, 1639
7 Van der Sanden, M. C. M., De Bie, F. O., Buijs, L. G. C. and Meijer, H. E. H. *Polymer* to be submitted
8 Sluijters, R. *De Ingenieur* 1965, **77** (15), 33
9 Schilo, D. and Ostertag, K. *Verfahrenstechnik* 1972, **6** (2), 45
10 Coumans, W. J. and Heikens, D. *Polymer* 1980, **21**, 957
11 Wu, S. *J. Polym. Sci., Polym. Phys. Edn.* 1987, **25**, 557
12 Wu, S. *J. Polym. Sci., Polym. Phys. Edn.* 1987, **25**, 2511
13 Ferry, J. D. 'Viscoelastic Properties of Polymers', Wiley, New York, 1980
14 Onogi, S., Masuda, T. and Kitagawa, K. *Macromolecules* 1970, **3**, 109
15 Van der Sanden, M. C. M. and Meijer, H. E. H. *Polymer* to be submitted
16 Kinloch, A. J. and Young, R. J. 'Fracture Behaviour of Polymers', Elsevier Applied Science, London, 1985
17 Maxwell, M. A. and Yee, A. F. *Polym. Eng. Sci.* 1981, **21** (4), 205
18 Bucknall, C. B. 'Toughened Plastics', Applied Science, London, 1977
19 Kramer, E. J. *Adv. Polym. Sci.* 1983, **51/52**, 1
20 Van der Sanden, M. C. M. and Meijer, H. E. H. *Polymer* submitted
21 Borggreve, R. J. M., Gaymans, R. J., Schuijer, J. and Ingen Housz, J. F. *Polymer* 1987, **28**, 1489
22 Wu, S. *Polymer* 1985, **26**, 1855
23 Wu, S. *J. Appl. Polym. Sci.* 1988, **35**, 549
24 Kambour, R. P. *Polym. Commun.* 1983, **24**, 292